BIOCHEMISTRY
including biophysical chemistry & molecular biology

Article

pubs.acs.org/biochemistry

Structural Basis of Substrate Recognition by Aldehyde Dehydrogenase 7A1

Min Luo[†] and John J. Tanner*[,†,‡]

[†]Department of Chemistry, University of Missouri—Columbia, Columbia, Missouri 65211, United States
[‡]Department of Biochemistry, University of Missouri—Columbia, Columbia, Missouri 65211, United States

ABSTRACT: Aldehyde dehydrogenase 7A1 (ALDH7A1) is part of lysine catabolism and catalyzes the NAD^+-dependent oxidation of α-aminoadipate semialdehyde to α-aminoadipate. Herein, we describe a structural study of human ALDH7A1 focused on substrate recognition. Five crystal structures and small-angle X-ray scattering data are reported, including the first crystal structure of any ALDH7 family member complexed with α-aminoadipate. The product binds with the ε-carboxylate in the oxyanion hole, the aliphatic chain packed into an aromatic box, and the distal end of the product anchored by electrostatic interactions with five conserved residues. This binding mode resembles that of glutamate bound to the proline catabolic enzyme ALDH4A1. Analysis of ALDH7A1 and ALDH4A1 structures suggests key interactions that underlie substrate discrimination. Structures of apo ALDH7A1 reveal dramatic conformational differences from the product complex. Product binding is associated with a 16 Å movement of the C-terminus into the active site, which stabilizes the active conformation of the aldehyde substrate anchor loop. The fact that the C-terminus is part of the active site was hitherto unknown. Interestingly, the C-terminus and aldehyde anchor loop are disordered in a new tetragonal crystal form of the apoenzyme, implying that these parts of the enzyme are highly flexible. Our results suggest that the active site of ALDH7A1 is disassembled when the aldehyde site is vacant, and the C-terminus is a mobile element that forms quaternary structural interactions that aid aldehyde binding. These results are relevant to the c.1512delG genetic deletion associated with pyridoxine-dependent epilepsy, which alters the C-terminus of ALDH7A1.

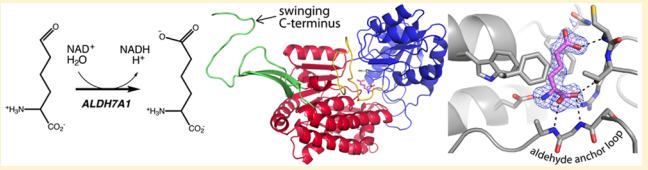

Aldehyde dehydrogenase 7A1 (ALDH7A1, also called antiquitin) plays a role in lysine catabolism by catalyzing the NAD^+-dependent oxidation of α-aminoadipate semialdehyde (AASA) to α-aminoadipate (AA) (Figure 1A). ALDH7A1 and other ALDHs are important biomarkers of cancer stem cells and play a functional role in cancer stem cell-mediated metastasis and cancer drug resistance.[1−6] Overexpression of ALDH1A1, ALDH1A3, ALDH2, ALDH4A1, and ALDH7A1 isoforms has been found in several types of cancers.[4] A high level of expression of ALDH7A1 occurs in prostate cancer cells lines, prostate cancer tissue, and matched bone metastasis samples, suggesting that ALDH7A1 plays a functional role in prostate cancer bone metastasis.[7] In addition, patients with ALDH7A1-expressing non-small cell lung carcinoma tumors have a significantly increased incidence of lung cancer recurrence,[8] and the level of ALDH7A1 expression is increased in ovarian tumors.[9]

Mutations in ALDH7A1 cause the inherited seizure disorder pyridoxine-dependent epilepsy (PDE).[10,11] PDE is an autosomal recessive epileptic encephalopathy caused by mutations in the gene encoding ALDH7A1.[10,11] PDE is characterized by intractable seizures that are not controlled with antiepileptic drugs but that respond to large daily supplements of pyridoxine, a form of vitamin B6. Disruption of ALDH7A1 activity in PDE patients causes a buildup of AASA, which forms a spontaneous equilibrium with Δ^1-piperideine-6-carboxylic acid (Figure 1B). The accumulating Δ^1-piperideine-6-carboxylic acid inactivates pyridoxal 5′-phosphate via Knoevenagel condensation (Figure 1B), leading to a pyridoxal 5′-phosphate deficiency.[10] Because pyridoxal 5′-phosphate is a cofactor in many enzymes, this chemically induced pyridoxal 5′-phosphate deficiency has major metabolic consequences, including changes in brain chemistry that lead to seizures. The mutational spectrum of PDE is very large. More than 60 different mutations within the 18 exons of the ALDH7A1 gene have been reported, including splice site mutations, insertions, deletions, nonsense mutations, and more than two dozen missense mutations.[11,12]

Herein, we describe a structural and biochemical study of ALDH7A1 focusing on substrate recognition and conformational change. We report the first structures of the full-length human enzyme, including the first structure of any ALDH7 family member complexed with the product AA. The structures show that the C-terminus is a mobile active site element that facilitates substrate recognition.

EXPERIMENTAL PROCEDURES

Crystallization of Apo ALDH7A1 in Space Group *C*2. Full-length recombinant human cytosolic ALDH7A1 isoform 2 (511 residues, NCBI RefSeq NP_001188306.1) was expressed and purified as described previously.[13]

Received: July 6, 2015
Revised: August 5, 2015
Published: August 11, 2015

DOI: 10.1021/acs.biochem.5b00754
Biochemistry 2015, 54, 5513−5522

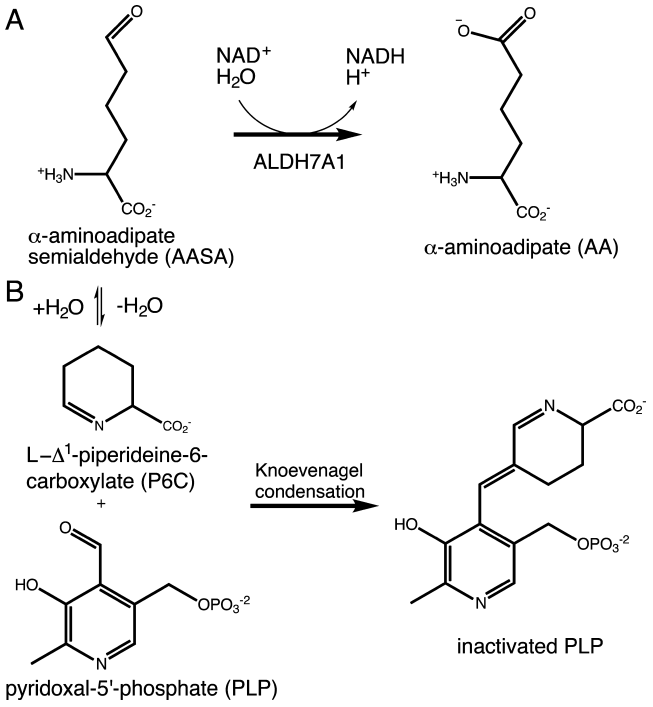

Figure 1. Reactions related to ALDH7A1 and PDE. (A) Reaction catalyzed by ALDH7A1. (B) Inactivation of pyridoxal 5′-phosphate by Δ^1-piperideine-6-carboxylic acid.

Centered monoclinic crystals of apo ALDH7A1 were grown in sitting drops (Crystal*EX* 96-well plates from Hampton Research) at 22 °C using drops formed by mixing 3 μL each of the protein and reservoir solutions. The protein stock solution contained 3 mg/mL ALDH7A1 in a buffer containing 50 mM Tris (pH 7.8), 0.5 mM tris(3-hydroxypropyl)phosphine (THP), 50 mM NaCl, and 5% glycerol (precrystallization buffer). The reservoir contained 0.2 M ammonium sulfate, 20% (w/v) polyethylene glycol (PEG) 3350, and 0.1 mM Bis-Tris (pH 6.5), which was obtained by optimizing a hit from crystal screening trials using commercially available kits (Hampton Research). The crystals were cryoprotected in the reservoir solution supplemented with 16% (v/v) PEG 200, picked up with Hampton nylon loops, and plunged into liquid nitrogen. The space group is *C*2 with the following unit cell dimensions: a = 157 Å, b = 163 Å, c = 160 Å, and β = 94°. The asymmetric unit includes eight protein molecules (two tetramers), which implies 46% solvent and a V_M of 2.29 Å^3/Da. We note that this is the same crystal form that was reported by Brocker et al. for ALDH7A1 complexed with NADH,[14] although the components of the crystallization solution are somewhat different and the construct that we used encodes the full 511-residue protein.

Cocrystallization of ALDH7A1 with NAD$^+$ in Space Group *C*2. Prior to crystallization, NAD$^+$ was added to the protein stock solution (3 mg/mL ALDH7A1) to a final concentration of 5 mM. Crystals of the ALDH7A1−NAD$^+$ complex were grown in sitting drops (Crystal*EX* 96-well plates) at 22 °C with the aid of streak microseeding. The microseed stock was prepared by crushing crystals of *C*2 apo ALDH7A1 in a buffer of 0.2 M ammonium sulfate, 20% (w/v) PEG 3350, and 0.1 mM Bis-Tris (pH 6.5). The reservoir contained 0.2 M ammonium sulfate, 20% (w/v) PEG 3350, and 0.1 mM Bis-Tris (pH 6.5). The crystals were cryoprotected in the reservoir solution supplemented with 2 mM NAD$^+$ and 16% (v/v) PEG 200, picked up with Hampton nylon loops, and plunged into liquid nitrogen. The space group is *C*2 with the following unit cell dimensions: a = 156 Å, b = 162 Å, c = 159 Å, and β = 95°. This crystal form is the same one that was described in the preceding paragraph for apo ALDH7A1.

Cocrystallization of ALDH7A1 with L-2-Aminoadipate in Space Group *C*2. L-2-Aminoadipate (AA) was purchased from Sigma-Aldrich (catalog no. A7275). A stock solution of 300 mM AA in 1 M HCl was prepared, and then AA was added to precrystallization buffer to a final concentration of 100 mM with the pH adjusted to 7.5. A volume of the 100 mM AA solution was mixed with an equal volume of a 6 mg/mL ALDH7A1 stock solution in precrystallization buffer supplemented with 1.5% DMSO. The pH of the resulting solution was adjusted to 7.5, and the solution was stored overnight at 4 °C. Although the enzyme/AA solution turned cloudy, it was nevertheless used in matrix microseeding crystal screening trials using commercially available kits (Hampton Research). The crystal screens were performed in sitting drops at 22 °C in Crystal*EX* 96 trays. The sitting drops were formed by mixing 3 μL each of the reservoir and protein solutions. The microseed stock for these trials was prepared by crushing crystals of *C*2 apo ALDH7A1 in a buffer consisting of 0.2 M ammonium sulfate, 20% (w/v) PEG 3350, and 0.1 mM Bis-Tris (pH 6.5). After the protein and reservoir solutions were mixed, the microseeds were added to the drops by streaking with a horsehair. Following optimization of hits from the crystal screening trials, the *C*2 crystal form described above was obtained using a reservoir consisting of 0.1 M $MgCl_2$, 0.1 M sodium acetate trihydrate, 0.1 M Tris-HCl (pH 8.0), and 20% (w/v) PEG 4000. The crystals were cryoprotected with 0.1 M $MgCl_2$, 0.1 M sodium acetate trihydrate, 0.1 M Tris-HCl (pH 8.0), 20% (w/v) PEG 4000, and 15% (v/v) PEG 200, picked up with Hampton nylon loops, and plunged into liquid nitrogen. The space group is *C*2 with the following unit cell dimensions: a = 154 Å, b = 163 Å, c = 159 Å, and β = 95°.

Crystallization of Apo ALDH7A1 in Space Group *P*42$_1$2 and Soaking with NAD$^+$. Tetragonal crystals of apo ALDH7A1 were grown using the sitting drop method of vapor diffusion (Crystal*EX* 96-well plates from Hampton Research) at 22 °C with drops formed by mixing 3 μL each of the protein and reservoir solutions. The protein stock solution consisted of 3 mg/mL ALDH7A1 in a buffer containing 50 mM Tris (pH 7.8), 0.5 mM THP, 50 mM NaCl, and 5% glycerol. The best crystals were grown in 0.1 M Hepes (pH 7.5), 0.1 M $MgCl_2$, and 20% (w/v) PEG 3350. The crystals were cryoprotected using the reservoir supplemented with 18% (v/v) PEG 200, picked up with Hampton nylon loops, and plunged into liquid nitrogen. The space group is $P42_12$ with the following unit cell dimensions: $a = b$ = 159 Å, and c = 80 Å. The asymmetric unit includes two protein molecules, which implies 46% solvent content and a V_M of 2.28 Å^3/Da. The ALDH7A1−NAD$^+$ complex was obtained by soaking apo tetragonal ALDH7A1 crystals with the cryobuffer containing 1 mM NAD$^+$.

X-ray Diffraction Data Collection, Phasing, and Refinement. X-ray diffraction data for *C*2 apo ALDH7A1 crystals were collected on Northeastern Collaborative Access Team beamline 24-ID-E at the Advanced Photon Source using a Q315r detector. The 2.4 Å resolution data set used for refinement consisted of 180 frames with an oscillation width of 1° per image, a detector distance of 310 mm, and an exposure time of 1 s per image.

DOI: 10.1021/acs.biochem.5b00754
Biochemistry 2015, 54, 5513−5522

Table 1. X-ray Diffraction Data Collection and Refinement of Monoclinic Structures[a]

	AA	NAD^+	apo
beamline	APS 19-ID-C	ALS 4.2.2	APS 24-ID-E
space group	*C*2	*C*2	*C*2
unit cell parameters	a = 154.4 Å	a = 155.7 Å	a = 157.0 Å
	b = 162.5 Å	b = 161.6 Å	b = 162.5 Å
	c = 158.7 Å	c = 158.9 Å	c = 160.0 Å
	β = 95.0°	β = 94.8°	β = 94.1°
wavelength	0.979	1.000	0.979
resolution (Å)	47.9−1.76 (1.79−1.76)	62.9−2.00 (2.03−2.00)	16.0−2.40 (2.44−2.40)
no. of observations	1405606	995590	559499
no. of unique reflections	381768	261450	153212
$R_{merge}(I)$	0.066 (0.657)	0.106 (1.050)	0.150 (0.313)
$R_{meas}(I)$	0.078 (0.773)	0.123 (1.224)	0.176 (0.370)
$R_{pim}(I)$	0.040 (0.404)	0.063 (0.626)	0.063 (0.626)
mean I/σ	12.3 (1.9)	12.7 (1.3)	6.3 (3.1)
mean $CC_{1/2}$	0.998 (0.682)	0.997 (0.632)	0.967 (0.874)
completeness (%)	99.4 (99.8)	99.5 (96.1)	98.2 (99.7)
multiplicity	3.7 (3.6)	3.8 (3.7)	3.7 (3.5)
no. of protein chains	8	8	8
no. of protein residues	4070	4062	4056
no. of protein atoms	30562	30440	29450
no. of AA atoms	88	–	–
no. of NAD^+ atoms	–	200	–
no. of water molecules	1899	1345	557
R_{cryst}	0.168 (0.261)	0.171 (0.288)	0.226 (0.243)
R_{free}[b]	0.206 (0.308)	0.218 (0.352)	0.275 (0.312)
rmsd for bond lengths (Å)	0.006	0.007	0.003
rmsd for bond angles (deg)	1.000	1.021	0.738
Ramachandran plot[c] (%)			
favored	96.97	96.91	96.93
outliers	0.25	0.20	0.02
all-atom Clashscore[c]	2.1	2.5	2.3
average *B* factor (Å^2)			
protein	24.5	30.0	37.4
AA	31.3	–	–
NAD^+	–	40.0	–
water	29.3	29.7	28.4
coordinate error (Å)[d]	0.20	0.24	0.36
PDB entry	4ZUL	4ZUK	4ZVW

[a]Values for the outer resolution shell of data are given in parentheses. [b]The 5% test set. [c]Generated with MolProbity via PHENIX refine. [d]Maximum likelihood-based coordinate error estimate reported by PHENIX refine.

X-ray diffraction data from monoclinic and tetragonal crystals of the ALDH7A1−NAD^+ complex were collected on beamline 4.2.2 at the Advanced Light Source using a Taurus-1 CMOS detector in shutterless mode. Each data set consisted of 1800 frames covering a total rotation range of 180° with the detector distance set to 240 mm. The total exposure times were 540 s for the *C*2 data set and 180 s for the tetragonal data set.

X-ray diffraction data for crystals of the ALDH7A1−AA complex and tetragonal apo ALDH7A1 were collected on Structural Biology Center beamline 19-ID-C at the Advanced Photon Source using a Q315r detector. The 1.76 Å resolution data set used for refinement of the ALDH7A1−AA complex consisted of 720 frames with an oscillation width of 0.25° per image, a detector distance of 230 mm, and an exposure time of 1 s per image. The 1.90 Å resolution data set used for refinement of tetragonal apo ALDH7A1 consisted of 360 frames with an oscillation width of 0.5° per image, a detector distance of 260 mm, and an exposure time of 1 s per image.

The data sets were processed with XDS[15] and AIMLESS[16] via CCP4i.[17] PHENIX[18] and COOT[19] were used for refinement and model building, respectively. Crystallographic structure refinements against the *C*2 data sets were initiated from the coordinates of truncated ALDH7A1 [Protein Data Bank (PDB) entry 2J6L].[14] Initial phases for the tetragonal data sets were determined using molecular replacement as implemented in PHASER[20] with a search model derived from a dimer of human ALDH7A1 (PDB entry 2J6L). MolProbity was used for structure validation.[21] Data collection and refinement statistics are listed in Tables 1 and 2.

Small-Angle X-ray Scattering (SAXS). SAXS experiments were performed at beamline 12.3.1 of the Advanced Light Source via the mail-in program.[22,23] Prior to data collection, an ALDH7A1 sample was passed through a Superdex 200 size exclusion column. The column buffer consisted of 50 mM Tris, 5% glycerol, 0.5 mM THP, and 50 mM NaCl (pH 7.8). Scattering intensities were measured at three nominal protein concentrations using exposure times of 0.5, 1.0, 3.0, and 6.0 s.

DOI: 10.1021/acs.biochem.5b00754
Biochemistry 2015, 54, 5513−5522

Table 2. X-ray Diffraction Data Collection and Refinement of Tetragonal Structures[a]

	apo	NAD^+
beamline	APS 19-ID-C	ALS 4.2.2
space group	$P42_12$	$P42_12$
unit cell parameters	a = 159.3 Å	a = 158.9 Å
	c = 79.8 Å	c = 79.4 Å
wavelength	0.979	1.000
resolution (Å)	46.0−1.90 (1.93−1.90)	53.0−1.90 (1.94−1.90)
no. of observations	1175993	1175225
no. of unique reflections	81138	80249
$R_{merge}(I)$	0.097 (1.209)	0.102 (1.445)
$R_{meas}(I)$	0.100 (1.256)	0.105 (1.504)
$R_{pim}(I)$	0.026 (0.336)	0.028 (0.411)
mean I/σ	20.9 (2.4)	23.7 (2.5)
mean $CC_{1/2}$	0.999 (0.743)	0.999 (0.697)
completeness (%)	99.8 (96.5)	99.7 (95.0)
multiplicity	14.5 (13.5)	14.6 (13.3)
no. of protein chains	2	2
no. of protein residues	948	946
no. of protein atoms	7076	6994
no. of NAD^+ atoms	–	23
no. of water molecules	312	385
R_{cryst}	0.169 (0.281)	0.182 (0.269)
R_{free}[b]	0.195 (0.329)	0.213 (0.305)
rmsd for bond lengths (Å)	0.007	0.007
rmsd for bond angles (deg)	0.973	0.967
Ramachandran plot[c] (%)		
favored	98.30	98.51
outliers	0.11	0.00
all-atom Clashscore[c]	1.3	2.2
average B factor (Å^2)		
protein	34.8	35.2
NAD^+	–	35.1
water	35.0	32.8
coordinate error (Å)[d]	0.19	0.20
PDB entry	4ZVX	4ZVY

[a]Values for the outer resolution shell of data are given in parentheses. [b]The 5% test set. [c]Generated with MolProbity via PHENIX refine. [d]Maximum likelihood-based coordinate error estimate reported by PHENIX refine.

Scattering curves collected from the protein samples were corrected for background scattering using intensity data collected from the Superdex 200 column effluent. Composite scattering curves for each protein concentration were generated with PRIMUS[24] by scaling and merging the background-corrected high-q region from the 3 s exposure with the low-q region from the 0.5 or 1.0 s exposure. PRIMUS was also used for Guinier analysis. Shape reconstruction calculations were performed with the sastbx.shapeup module of the Small Angle Scattering ToolBox server.[25] The shape reconstruction calculations employed the PISA database of shapes. The FoXS server was used to calculate SAXS profiles from atomic coordinates.[26]

RESULTS

ALDH7A1 Adopts the Standard ALDH Superfamily Fold. Crystal structures of ALDH7A1 were determined in space groups $C2$ (Table 1) and $P42_12$ (Table 2). ALDH7A1 exhibits the ALDH superfamily fold consisting of NAD^+-binding, catalytic, and oligomerization domains (Figure 2A).

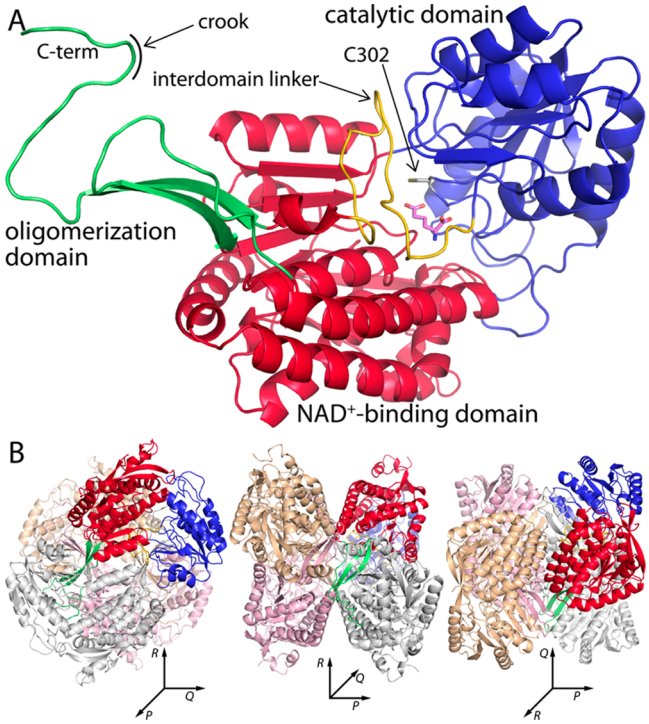

Figure 2. Structure of ALDH7A1. (A) Protomer structure of ALDH7A1 highlighting domain architecture. The three domains are colored red (NAD^+-binding), blue (catalytic), and green (oligomerization). One of the polypeptide sections that links the catalytic and NAD^+-binding domains is colored gold. AA is colored pink. (B) Three orthogonal views of the ALDH7A1 dimer-of-dimers tetramer. One protomer is colored according to domains as in panel A, while the other three protomers each have a different color (gray, pink, or wheat). The three orientations correspond to viewing along the three mutually perpendicular 2-fold axes of the tetramer, which are labeled P, Q, and R.

The NAD^+-binding domain adopts the Rossmann fold. As in other ALDHs, the core of this domain is a parallel five-stranded β-sheet having a 32145 strand order. This topology differs from the classic Rossmann fold sheet, which has six strands arranged in a 321456 strand order. The catalytic domain has an α/β structure and contains the nucleophilic Cys302 residue that attacks the carbonyl of the aldehyde substrate. The oligomerization domain is a β-substructure that mediates domain-swapped dimerization. The active site is located in the crevice between the NAD^+-binding and catalytic domains.

Two sections of the polypeptide chain link the NAD^+-binding and catalytic domains. These sections are notable because they form part of the active site. The short linker consisting of residues 269−271 connects strand 5 of the Rossmann sheet to the beginning of the catalytic domain. This linker interacts with the carboxamide of the cofactor.[14] The

DOI: 10.1021/acs.biochem.5b00754
Biochemistry 2015, 54, 5513−5522

other linker is longer and consists of residues 461−482 (yellow in Figure 2A). As described below, this linker interacts with the product AA and adopts multiple conformations.

ALDH7A1 Forms the Classic ALDH Dimer-of-Dimers Tetramer in Solution. Small-angle X-ray scattering (SAXS) was used to determine the oligomeric state and quaternary structure of ALDH7A1 in solution. Guinier analysis of three ALDH7A1 samples having different protein concentrations yields a radius of gyration (R_g) of 37.7 ± 0.3 Å (Figure 3A).

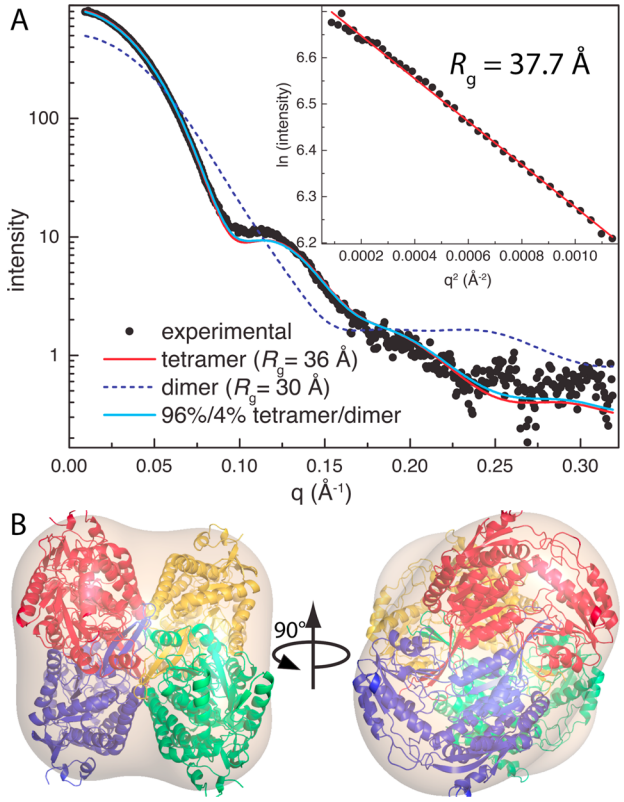

Figure 3. SAXS analysis of ALDH7A1. (A) Comparison of the experimental SAXS curve with those calculated from ALDH7A1 oligomers using FoXS.[26] The fits have χ values of 1.5 for the tetramer, 12.4 for the dimer, and 1.2 for the 96%/4% tetramer/dimer ensemble. The inset shows a Guinier plot, which spans the qR_g range of 0.356−1.273. (B) Superposition of the ALDH7A1 tetramer with the envelope from shape reconstruction calculations.

ALDHs are known to form domain-swapped dimers, and in some cases, the dimers assemble into tetramers[27] or hexamers.[28,29] The classic ALDH tetramer is present in both the *C*2 and $P42_12$ lattices (Figure 2B). The tetramer is a dimer of dimers having 222 symmetry, which can be described by three mutually perpendicular 2-fold axes (Figure 2B). This tetramer is also present in the *F*222 and *I*422 crystal forms of covalently inactivated ALDH7A1 that we recently reported.[13] The R_g calculated from the ALDH7A1 tetramer is 36 Å, which is close to the experimental SAXS value of 37.7 Å. In contrast, the dimer has an R_g of only 30 Å, while hexameric ALDHs have an R_g of 43 Å. Thus, analysis of R_g and crystal packing suggests that ALDH7A1 is tetrameric in solution.

Additional analysis of the SAXS data also indicates a tetramer in solution. The SAXS curve calculated from the tetramer has good agreement with the experimental curve (χ = 1.5), while that calculated from a domain-swapped dimer shows large deviations (χ = 12.4) (Figure 3A). Multiple Ensemble Search analysis[30] marginally improves the fit (χ = 1.2) and indicates 96% tetramer and 4% dimer. Also, the tetramer is consistent with the SAXS shape reconstruction (Figure 3B). In summary, SAXS suggests that ALDH7A1 forms the classic ALDH dimer-of-dimers tetramer in solution, which is also observed for ALDH1 and ALDH2.[27]

The Structure of ALDH7A1 Complexed with AA Provides Insight into Substrate Recognition. The structure of ALDH7A1 complexed with the product AA was determined at 1.76 Å resolution (Table 1). The active site is located in the crevice between the NAD^+-binding and catalytic domains, below the long interdomain linker peptide (Figure 2A). Catalytic Cys302 is torsioned away from AA and not in the nucleophilic attack rotamer, which is consistent with the presence of the product AA and the absence of NAD^+ (Figure 4).

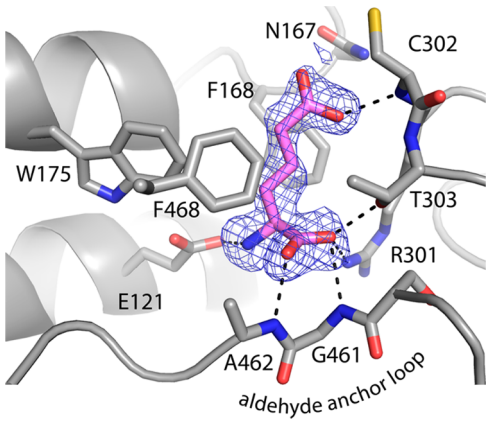

Figure 4. Electron density and interactions of AA bound to ALDH7A1. The mesh represents a simulated annealing $F_0 - F_c$ omit map contoured at 2.5σ.

AA forms several interactions with the enzyme (Figure 4). One of the oxygen atoms of the ε-carboxylate of AA occupies the oxyanion hole, forming a hydrogen bond with the backbone of catalytic Cys302. This atom represents the carbonyl O of the substrate AASA. Notably, this O atom apparently does not hydrogen bond with the conserved oxyanion hole residue Asn167, as the potential hydrogen bond distance is 3.9 Å. At the α-carbon end of the product, the carboxylate of AA is anchored by hydrogen bonds to the main chain of Gly461-Ala462 of the interdomain linker, another hydrogen bond with Thr303, and an ion pair with Arg301. The amino group of AA forms an ion pair with Glu121. The aliphatic chain of AA packs into an aromatic box formed by Phe168, Trp175, and Phe468. We note that aromatic boxes are often found in ALDH active sites.[31]

The product is essentially inaccessible to solvent. Calculations of the solvent accessibility with CNS[32] show that the product exposes only 2% of its total surface area when bound to the enzyme. This result indicates that AA is buried inside the protein and implies that protein conformational changes must occur to release the product. As described below, this conformational change likely involves the C-terminus.

The C-Terminus Contributes to the Active Site through Quaternary Structural Interactions. The AA complex structure shows that the C-terminus plays a role in stabilizing the active site. The 13 C-terminal residues form an

DOI: 10.1021/acs.biochem.5b00754
Biochemistry 2015, 54, 5513−5522

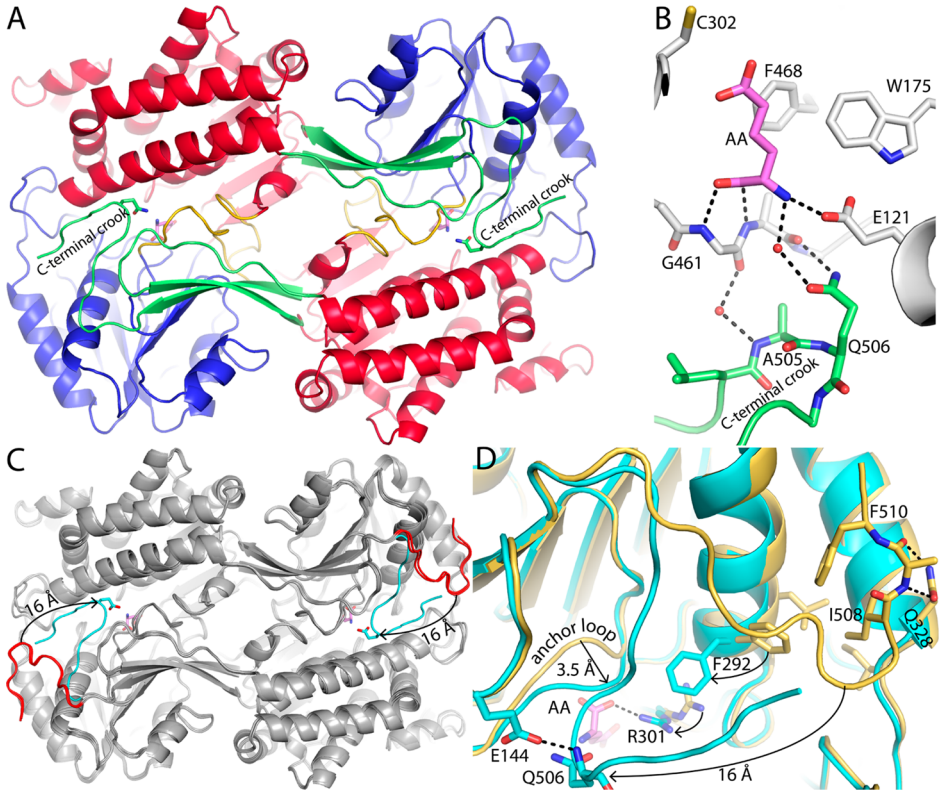

Figure 5. Conformational variation of the C-terminus. (A) Dimer of ALDH7A1 complexed with AA (pink). The domains are colored as in Figure 2A, with the NAD$^+$-binding domain colored red, the catalytic domain blue, and the oligomerization domain green. Gln506 is shown as sticks. (B) Close-up of the quaternary structural interactions that stabilize the aldehyde-binding site in the AA complex. One protomer of the dimer is colored white with bound AA colored pink. The C-terminus of the other protomer is colored green. (C) Superposition of the dimers of the ALDH7A1−AA complex (gray with a cyan C-terminus), apo ALDH7A1 in space group *C*2 (gray with a red C-terminus), and the ALDH7A1−NAD$^+$ complex in space group *C*2 (also gray with a red C-terminus). The arrow indicates the 16 Å movement of the C-terminus from the open conformation (AA-free) to the closed conformation (AA-bound). (D) Close-up of a superposition of the AA complex (cyan) and the apoenzyme in space group *C*2 (gold). The arrows indicate movement of the active site from the open conformation (AA-free) to the closed conformation (AA-bound). AA is colored pink.

L-shaped appendage that is connected to the final β-strand of the oligomerization domain (Figure 2A). In the domain-swapped dimers that make up the tetramer, this appendage forms quaternary structural interactions with the catalytic and NAD$^+$-binding domains (Figure 5A). In particular, the crook of the appendage of one protomer interacts with the active site of another protomer. For example, Gln506 of the crook forms a water-mediated hydrogen bond to the amino group of AA (Figure 5B). Also, Glu506 and Ala505 appear to stabilize the aldehyde anchor loop (residues 461−463). Glu506 hydrogen bonds to Ala462, while the methyl group of Ala505 packs tightly against residues 461−463. These interactions may facilitate substrate recognition, because the anchor loop forms hydrogen bonds with the C-1 carboxylate of AA (Figure 5B and Figure 4).

The Active Site Conformation Is Variable in the Absence of AA. The structures of ALDH7A1 without bound AA were determined to gain insight into the conformational flexibility of the active site. Structures of the apoenzyme and the NAD$^+$ complex were determined in the same *C*2 lattice as the AA complex and also in space group $P42_12$ (Tables 1 and 2).

NAD$^+$ binds in the expected location at the C-termini of the strands of the Rossmann fold domain. Electron density is strong for the AMP portion of the cofactor but weak and variable for the nicotinamide half of the cofactor. Accordingly, the nicotinamide riboside could not be modeled in any of the protomers of the two NAD$^+$ complex structures. We note that density for the nicotinamide of NAD$^+$ bound to maize ALDH7 is also weak[33] (PDB entry 4PXN), but the entire cofactor is ordered in a structure of truncated human ALDH7A1 complexed with NADH (PDB entry 2J6L). Disorder of the nicotinamide half of the cofactor has been observed in other ALDHs.[34,35]

The conformation of the C-terminus appears to be highly variable in the absence of AA. In the *C*2 apo enzyme and *C*2 NAD$^+$ complex, the C-terminus is rotated out of the active site (Figure 5C). Compared to the AA complex, the crook of the C-terminus shifts by 16 Å, which leaves the active site open and solvent-exposed. Intermolecular interactions appear to stabilize the open conformation of the C-terminus. Ile508 and Phe510 pack into a hydrophobic pocket located between two helices of the Rossmann fold domain, while the backbone of Lys509 forms two hydrogen bonds with the side chain of Gln328 (Figure 5D).

Comparison of the structures reveals additional differences between the closed (AA-bound) and open (AA-free) active sites (Figure 5D). In the open state, Phe292, Arg301, and the aldehyde anchor loop are displaced from the active site. In the closed state, Phe292 has rotated into the space occupied by Arg301 of the open state, while Arg301 and the anchor loop converge to engage the carboxylate of AA. Hydrogen bonds to the backbone of the C-terminus also differ in the two active site

DOI: 10.1021/acs.biochem.5b00754
Biochemistry 2015, 54, 5513−5522

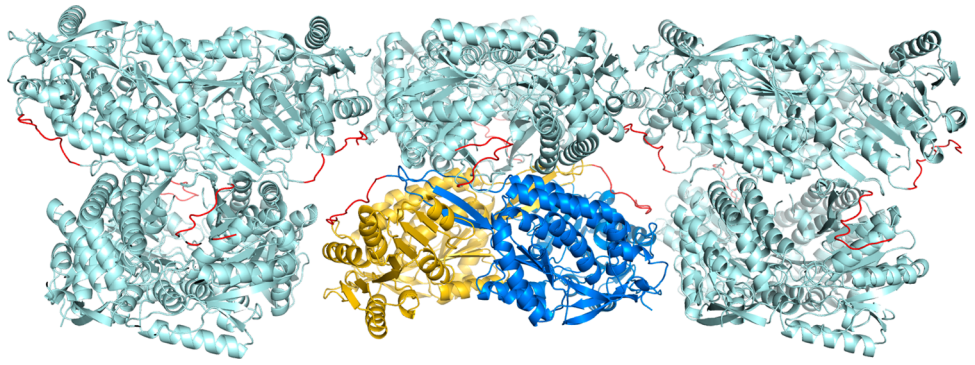

Figure 6. Crystal packing of ALDH7A1 in $P42_12$. The lattice is viewed down the *a*-axis, with the *b*-axis horizontal and *c*-axis vertical. The two chains of the asymmetric unit are colored gold and blue. Neighboring chains are colored pale cyan. The C-terminus from the *C*2 structure (open conformation) has been grafted onto the $P42_12$ structure and is colored red. Note that the modeled C-terminus occupies a solvent channel.

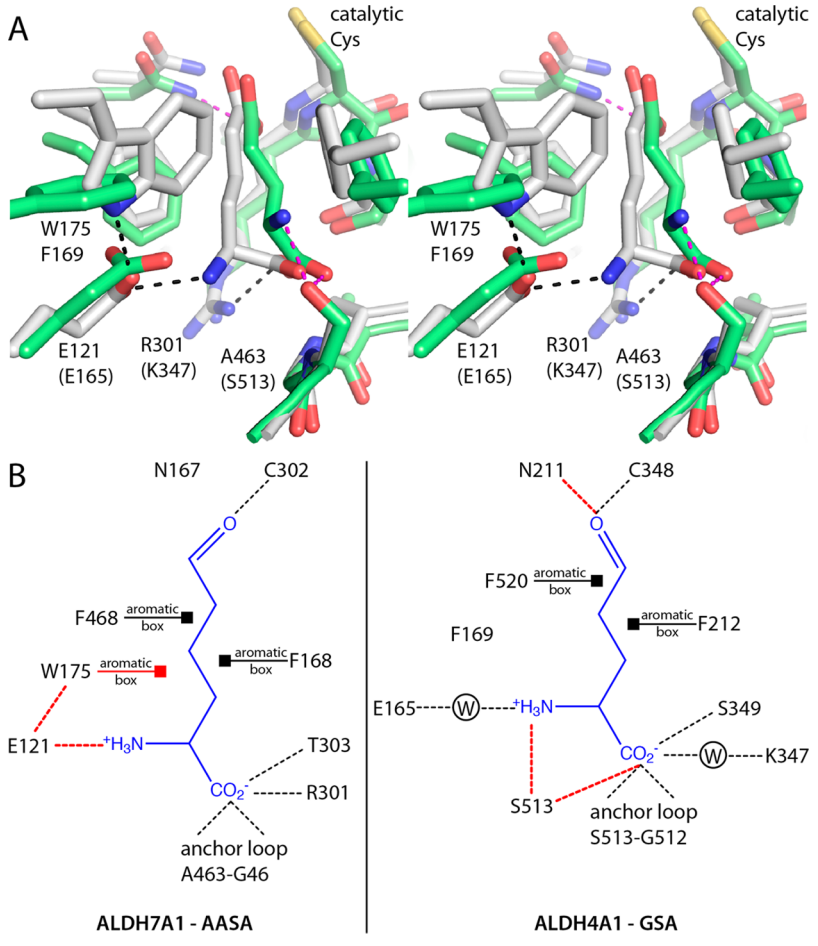

Figure 7. Comparison of substrate recognition in ALDH7A1 and ALDH4A1. (A) Superposition of ALDH7A1 complexed with AA (white) and ALDH4A1 complexed with Glu (green). Black dashes indicate interactions that are unique to ALDH7A1. Magenta dashes denote those unique to ALDH4A1. (B) Substrate interaction diagrams for ALDH7A1 and ALDH4A1 inferred from the enzyme−product complex structures. Dashes denote hydrogen bonds and ion pairs. Squares denote van der Waals interactions between aromatic box residues and the aliphatic chain of the substrate. Interactions unique to either enzyme are colored red. W in a circle represents water-mediated interactions.

conformations. As noted above, the open conformation is stabilized by intermolecular hydrogen bonding between Lys509 and Gln328. Upon closure, these interactions are broken, and a new intramolecular hydrogen bond between the backbone of Gln506 and the side chain of Glu144 is formed (Figure 5D).

The tetragonal structures, which were determined in the absence of bound AA, suggest a more severe conformational variation of the active site. In these structures, electron density for the 12 C-terminal residues (500−511) is absent in both chains in the asymmetric unit. Similarly, electron density for the long interdomain linker (residues 459−481) is missing. The absence of these parts of the structure leaves the active site disassembled and highly solvent-exposed. The disordered sections are notable because they contain residues that bind AA, including the anchor loop, the crook of the C-terminus, and aromatic box residue Phe468.

DOI: 10.1021/acs.biochem.5b00754
Biochemistry 2015, 54, 5513−5522

The two ALDH7A1 crystal lattices were analyzed to understand the influence of crystal packing on the conformation and disorder of the C-terminus. In particular, we wondered whether crystal packing in space group *C*2 artificially stabilizes the C-terminus. This analysis showed that the C-terminus is free of crystal contacts (5.0 Å cutoff). This result is consistent with the fact that the *C*2 lattice accommodates both the open and closed conformations, which differ by as much as 16 Å (Figure 5C). We also entertained the possibility that steric hindrance in space group $P42_12$ prevents the C-terminus from adopting the conformations observed in the *C*2 structure. This idea was tested by grafting the C-terminus from the *C*2 structure (open conformation) onto the $P42_12$ structure and inspecting the crystal packing interactions in the hypothetical structure. The grafted C-terminus extends into a solvent channel between two tetramers and does not clash with neighboring molecules in the lattice (Figure 6). Thus, the $P42_12$ lattice seems to be compatible with the open (and closed) conformation of the C-terminus. The absence of electron density implies that the C-terminus adopts multiple conformations in the $P42_12$ crystal. Apparently, the solvent channel is large enough to accommodate multiple, diverse conformations of the C-terminus.

Comparison to ALDH4A1. ALDH4A1 and ALDH7A1 recognize structurally similar substrates. ALDH4A1 is the last enzyme in the proline catabolic pathway and catalyzes the oxidation of glutamate-γ-semialdehyde (GSA) to glutamate. GSA and AASA are nearly isostructural, differing by just one extra methylene group in the aliphatic chain of AASA. Because we had previously determined the structure of ALDH4A1 complexed with the product glutamate (PDB entry 3V9K),[34] we decided to compare that structure to that of the ALDH7A1−AA complex to understand how these enzymes discriminate between closely related substrates.

The active sites of ALDH7A1 and ALDH4A1 are very similar in terms of amino acid composition and structure, despite sharing only 24% global sequence identity (Figure 7). Several active site residues are identically conserved: the Asn residue of the oxyanion hole, two Phe residues of the aromatic box, a Gly in the anchor loop, and a Glu near the substrate amino group. Two conservative substitutions are also evident: Arg301 and Thr303 of ALDH7A1 correspond to Lys347 and Ser349 of ALDH4A1, respectively.

The active sites also have two notable sequence differences that may facilitate discrimination between AASA and GSA (Figure 7). First, Ala463 in the anchor loop of ALDH7A1 is replaced with Ser513 in ALDH4A1. Ser513 forms hydrogen bonds with the amino group and the α-carboxylate of the product in ALDH4A1. Second, the aromatic box residue Trp175 of ALDH7A1 corresponds to Phe169 of ALDH4A1. The bulkier Trp175 contacts the aliphatic chain of AA, whereas Phe169 is too small for such interaction with glutamate in ALDH4A1. Furthermore, the indole of Trp175 forms a hydrogen bond with Glu121, which in turn ion pairs to the amino group of AA. It thus appears that Trp175 positions Glu121 for ion pairing with AA. Because of these structural differences, the amino group is situated 3 Å closer to the anchor loop in ALDH4A1, which allows hydrogen bonding with Ser513 and prevents ion pairing with Glu165.

DISCUSSION

The fact that the C-terminus is part of the active site of ALDH7A1 was hitherto unknown. This feature has not been described because the previous structural study of human ALDH7A1 used a truncated construct that lacks the final 12 amino acid residues.[14] Also, a structure of maize ALDH7 was recently reported; however, the crystalline enzyme lacks a ligand in the aldehyde site, so the C-terminus is retracted as in our apo *C*2 structure.[33]

Our structures show that the C-terminus of ALDH7A1 adopts multiple conformations, including an L-shaped structure that swings between opened and closed positions (Figure 5C), and other unresolved conformations that are implied by the $P42_12$ structure in which the C-terminus is disordered. In the closed state, the C-terminus of one protomer stabilizes the aldehyde-binding site of another protomer. The close approach of the crook of the C-terminus to the aldehyde anchor loop suggests that the C-terminus plays a role in aldehyde binding and product release. In particular, Ala505 packs against the anchor loop and forms a water-mediated interaction with anchor loop residue Gly461, while Gln506 hydrogen bonds directly to aldehyde anchor loop residue Ala462 and indirectly to AA (Figure 5B). We note that Gly461, Ala462, Ala505, and Gln506 are identically conserved in family 7 of the ALDH superfamily, which includes enzymes from diverse organisms that are related by as little as 50% global sequence identity. The observed interactions among these residues and their strong conservation imply a functionally important role, which we suggest is aldehyde substrate recognition.

Our structures and proposed role for the C-terminus in AASA recognition are consistent with the generally accepted mechanism of ALDHs[36] in which NAD^+ binds before the aldehyde substrate. The C-terminus of the NAD^+ complex adopts the open state conformation (*C*2 form) or is disordered ($P42_12$). Thus, the aldehyde-binding site is accessible when NAD^+ is bound, which allows formation of the ternary enzyme−NAD^+−AASA complex. In summary, our structures are consistent with the C-terminus being a dynamic active site element that facilitates the binding of AASA.

The discovery that the C-terminus of ALDH7A1 is part of the active site aids our understanding of the c.1512delG genetic deletion, which is implicated in PDE.[10] Deletion of G1512 from exon 18 mutates six of the last seven amino acids of the wild-type polypeptide and extends the C-terminus by 10 residues (Figure 8). It is possible that the mutated C-terminus is

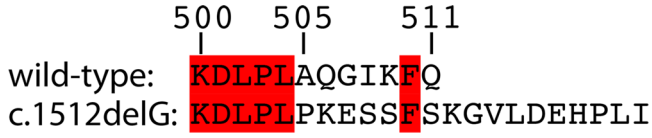

Figure 8. Sequence alignment of the C-termini of wild-type ALDH7A1 and the c.1512delG deletion mutant, which has been implicated in PDE.

incapable of forming the closed state that we observed in the AA complex structure. If so, the mutation may cause a defect in AASA recognition, which would impact catalytic function. In particular, c.1512delG changes the crook residues Ala505 and Gln506 to Pro and Lys, respectively. Mutation of Ala505 to Pro may alter the L shape and reduce the flexibility of the C-terminus, and the longer lysine side chain at position 506 may be unable to interact favorably with AASA or the anchor loop. Also, because the C-terminus forms quaternary structural interactions, it is possible that c.1512delG affects oligomerization. The longer C-terminus could also affect protein solubility.

DOI: 10.1021/acs.biochem.5b00754
Biochemistry 2015, 54, 5513−5522

Site-directed mutagenesis of recombinant ALDH7A1 could be used to improve our understanding of the structural and biochemical consequences of c.1512delG.

The AA complex structure permitted an examination of how ALDH7A1 and ALDH4A1 discriminate between the structurally similar substrates AASA and GSA. These two substrates differ only in the number of methylene groups. Our analysis suggests that ALDH7A1 and ALDH4A1 accommodate the different aliphatic chain lengths by modulating the position of the distal end of the substrate, with the amino group shifted 3 Å closer to the anchor loop in ALDH4A1 (Figure 7A). Two residues appear to underlie this subtle difference in substrate pose: Ala/Ser in the aldehyde anchor loop and Trp/Phe in the aromatic box. One may be able to alter the substrate specificities of ALDH7A1 and ALDH4A1 by mutating these residues.

Finally, the tetragonal structure of ALDH7A1 provides another example of an ALDH crystal structure with a disordered active site. Electron density is lacking for the interdomain linker and C-terminus in the two tetragonal ALDH7A1 structures. The interdomain linker is also disordered in structures of human and yeast ALDH4A1[29] (PDB entries 4OE6 and 4OE5) and ALDH1A2 (PDB entry 1BI9).[37,38] This disorder is significant because the interdomain linker contains the aldehyde anchor loop and one of the aromatic box residues (Figure 4). The interpretation of these disordered structures is not obvious. Perhaps they indicate that the interdomain linker is highly flexible and samples multiple conformations when the aldehyde site is vacant. This interpretation is consistent with a conformational selection mechanism[39] of substrate recognition. With the list of ALDHs exhibiting disordered active sites growing, it may be worthwhile to consider whether this phenomenon is a global aspect of the superfamily.

■ ASSOCIATED CONTENT

Accession Codes

Atomic coordinates and structure factor amplitudes have been deposited in the Protein Data Bank as entries 4ZUL (AA complex), 4ZUK (*C*2 NAD^+ complex), 4ZVW (*C*2 apo), 4ZVX ($P42_12$ apo), and 4ZVY ($P42_12$ NAD^+ complex).

■ AUTHOR INFORMATION

Corresponding Author

*Department of Biochemistry, University of Missouri—Columbia, Columbia, MO 65211. E-mail: tannerjj@missouri.edu. Phone: (573) 884-1280. Fax: (573) 882-2754.

Funding

Research reported in this publication was supported by the National Institute of General Medical Sciences of the National Institutes of Health via Grant GM065546.

Notes

The authors declare no competing financial interest.

■ ACKNOWLEDGMENTS

We thank Kevin Dyer for collecting the SAXS data through the SIBYLS mail-in program. We thank Dr. Jay Nix of Advanced Light Source beamline 4.2.2, Dr. Jonathan Schuermann of the Northeastern Collaborative Access Team, and Dr. Norma Duke of the Structural Biology Center for help with X-ray diffraction data collection and processing. Part of the research was performed at the Advanced Light Source, which is supported by the Director, Office of Science, Office of Basic Energy Sciences, of the U.S. Department of Energy (DOE) under Contract DE-AC02-05CH11231. The Advanced Light Source is a national user facility operated by Lawrence Berkeley National Laboratory on behalf of the Department of Energy, Office of Basic Energy Sciences, through the Integrated Diffraction Analysis Technologies (IDAT) program, supported by the DOE Office of Biological and Environmental Research. Additional support comes from the National Institute of Health Project MINOS (R01GM105404). Results shown in this report are derived in part from work performed at Argonne National Laboratory, Structural Biology Center, at the Advanced Photon Source. Part of this work is based upon research conducted at the Northeastern Collaborative Access Team beamlines, which are funded by the National Institute of General Medical Sciences from the National Institutes of Health (P41 GM103403). This research used resources of the Advanced Photon Source, a U.S. Department of Energy (DOE) Office of Science User Facility operated for the DOE Office of Science by Argonne National Laboratory under Contract DE-AC02-06CH11357.

■ ABBREVIATIONS

ALDH, aldehyde dehydrogenase; AASA, α-aminoadipate semialdehyde; AA, α-aminoadipate; PDE, pyridoxine-dependent epilepsy; THP, tris(3-hydroxypropyl)phosphine; SAXS, small-angle X-ray scattering; GSA, glutamate-γ-semialdehyde.

■ REFERENCES

(1) Abdullah, L. N., and Chow, E. K. (2013) Mechanisms of chemoresistance in cancer stem cells. *Clin. Transl. Med. 2*, 3.

(2) Januchowski, R., Wojtowicz, K., and Zabel, M. (2013) The role of aldehyde dehydrogenase (ALDH) in cancer drug resistance. *Biomed. Pharmacother. 67*, 669−680.

(3) Ma, I., and Allan, A. L. (2011) The role of human aldehyde dehydrogenase in normal and cancer stem cells. *Stem. Cell. Rev. 7*, 292−306.

(4) Marcato, P., Dean, C. A., Giacomantonio, C. A., and Lee, P. W. (2011) Aldehyde dehydrogenase: its role as a cancer stem cell marker comes down to the specific isoform. *Cell Cycle 10*, 1378−1384.

(5) Muzio, G., Maggiora, M., Paiuzzi, E., Oraldi, M., and Canuto, R. A. (2012) Aldehyde dehydrogenases and cell proliferation. *Free Radical Biol. Med. 52*, 735−746.

(6) Vasiliou, V., Thompson, D. C., Smith, C., Fujita, M., and Chen, Y. (2013) Aldehyde dehydrogenases: from eye crystallins to metabolic disease and cancer stem cells. *Chem.-Biol. Interact. 202*, 2−10.

(7) van den Hoogen, C., van der Horst, G., Cheung, H., Buijs, J. T., Pelger, R. C., and van der Pluijm, G. (2011) The aldehyde dehydrogenase enzyme 7A1 is functionally involved in prostate cancer bone metastasis. *Clin. Exp. Metastasis 28*, 615−625.

(8) Giacalone, N. J., Den, R. B., Eisenberg, R., Chen, H., Olson, S. J., Massion, P. P., Carbone, D. P., and Lu, B. (2013) ALDH7A1 expression is associated with recurrence in patients with surgically resected non-small-cell lung carcinoma. *Future Oncol. 9*, 737−745.

(9) Saw, Y. T., Yang, J., Ng, S. K., Liu, S., Singh, S., Singh, M., Welch, W. R., Tsuda, H., Fong, W. P., Thompson, D., Vasiliou, V., Berkowitz, R. S., and Ng, S. W. (2012) Characterization of aldehyde dehydrogenase isozymes in ovarian cancer tissues and sphere cultures. *BMC Cancer 12*, 329.

(10) Mills, P. B., Struys, E., Jakobs, C., Plecko, B., Baxter, P., Baumgartner, M., Willemsen, M. A., Omran, H., Tacke, U., Uhlenberg, B., Weschke, B., and Clayton, P. T. (2006) Mutations in antiquitin in individuals with pyridoxine-dependent seizures. *Nat. Med. 12*, 307−309.

(11) Stockler, S., Plecko, B., Gospe, S. M., Jr., Coulter-Mackie, M., Connolly, M., van Karnebeek, C., Mercimek-Mahmutoglu, S., Hartmann, H., Scharer, G., Struijs, E., Tein, I., Jakobs, C., Clayton,

DOI: 10.1021/acs.biochem.5b00754
Biochemistry 2015, 54, 5513−5522

P., and Van Hove, J. L. (2011) Pyridoxine dependent epilepsy and antiquitin deficiency: clinical and molecular characteristics and recommendations for diagnosis, treatment and follow-up. *Mol. Genet. Metab. 104*, 48−60.
(12) Scharer, G., Brocker, C., Vasiliou, V., Creadon-Swindell, G., Gallagher, R. C., Spector, E., and Van Hove, J. L. (2010) The genotypic and phenotypic spectrum of pyridoxine-dependent epilepsy due to mutations in ALDH7A1. *J. Inherited Metab. Dis. 33*, 571−581.
(13) Luo, M., Gates, K. S., Henzl, M. T., and Tanner, J. J. (2015) Diethylaminobenzaldehyde is a covalent, irreversible inactivator of ALDH7A1. *ACS Chem. Biol. 10*, 693−697.
(14) Brocker, C., Lassen, N., Estey, T., Pappa, A., Cantore, M., Orlova, V. V., Chavakis, T., Kavanagh, K. L., Oppermann, U., and Vasiliou, V. (2010) Aldehyde dehydrogenase 7A1 (ALDH7A1) is a novel enzyme involved in cellular defense against hyperosmotic stress. *J. Biol. Chem. 285*, 18452−18463.
(15) Kabsch, W. (2010) XDS. *Acta Crystallogr., Sect. D: Biol. Crystallogr. 66*, 125−132.
(16) Evans, P. R., and Murshudov, G. N. (2013) How good are my data and what is the resolution? *Acta Crystallogr., Sect. D: Biol. Crystallogr. D69*, 1204−1214.
(17) Potterton, E., Briggs, P., Turkenburg, M., and Dodson, E. (2003) A graphical user interface to the CCP4 program suite. *Acta Crystallogr., Sect. D: Biol. Crystallogr. D59*, 1131−1137.
(18) Afonine, P. V., Grosse-Kunstleve, R. W., Echols, N., Headd, J. J., Moriarty, N. W., Mustyakimov, M., Terwilliger, T. C., Urzhumtsev, A., Zwart, P. H., and Adams, P. D. (2012) Towards automated crystallographic structure refinement with phenix.refine. *Acta Crystallogr., Sect. D: Biol. Crystallogr. 68*, 352−367.
(19) Emsley, P., Lohkamp, B., Scott, W. G., and Cowtan, K. (2010) Features and development of Coot. *Acta Crystallogr., Sect. D: Biol. Crystallogr. 66*, 486−501.
(20) McCoy, A. J., Grosse-Kunstleve, R. W., Adams, P. D., Winn, M. D., Storoni, L. C., and Read, R. J. (2007) Phaser crystallographic software. *J. Appl. Crystallogr. 40*, 658−674.
(21) Chen, V. B., Arendall, W. B., 3rd, Headd, J. J., Keedy, D. A., Immormino, R. M., Kapral, G. J., Murray, L. W., Richardson, J. S., and Richardson, D. C. (2010) MolProbity: all-atom structure validation for macromolecular crystallography. *Acta Crystallogr., Sect. D: Biol. Crystallogr. D66*, 12−21.
(22) Hura, G. L., Menon, A. L., Hammel, M., Rambo, R. P., Poole, F. L., 2nd, Tsutakawa, S. E., Jenney, F. E., Jr., Classen, S., Frankel, K. A., Hopkins, R. C., Yang, S. J., Scott, J. W., Dillard, B. D., Adams, M. W., and Tainer, J. A. (2009) Robust, high-throughput solution structural analyses by small angle X-ray scattering (SAXS). *Nat. Methods 6*, 606−612.
(23) Classen, S., Hura, G. L., Holton, J. M., Rambo, R. P., Rodic, I., McGuire, P. J., Dyer, K., Hammel, M., Meigs, G., Frankel, K. A., and Tainer, J. A. (2013) Implementation and performance of SIBYLS: a dual endstation small-angle X-ray scattering and macromolecular crystallography beamline at the Advanced Light Source. *J. Appl. Crystallogr. 46*, 1−13.
(24) Konarev, P. V., Volkov, V. V., Sokolova, A. V., Koch, M. H. J., and Svergun, D. I. (2003) PRIMUS: a Windows PC-based system for small-angle scattering data analysis. *J. Appl. Crystallogr. 36*, 1277−1282.
(25) Liu, H., Hexemer, A., and Zwart, P. H. (2012) The Small Angle Scattering ToolBox (SASTBX): an open-source software for biomolecular small-angle scattering. *J. Appl. Crystallogr. 45*, 587−593.
(26) Schneidman-Duhovny, D., Hammel, M., and Sali, A. (2010) FoXS: a web server for rapid computation and fitting of SAXS profiles. *Nucleic Acids Res. 38*, W540−544.
(27) Rodriguez-Zavala, J. S., and Weiner, H. (2002) Structural aspects of aldehyde dehydrogenase that influence dimer-tetramer formation. *Biochemistry 41*, 8229−8237.
(28) Luo, M., Singh, R. K., and Tanner, J. J. (2013) Structural determinants of oligomerization of delta(1)-pyrroline-5-carboxylate dehydrogenase: identification of a hexamerization hot spot. *J. Mol. Biol. 425*, 3106−3120.
(29) Pemberton, T. A., Srivastava, D., Sanyal, N., Henzl, M. T., Becker, D. F., and Tanner, J. J. (2014) Structural Studies of Yeast Delta(1)-Pyrroline-5-carboxylate Dehydrogenase (ALDH4A1): Active Site Flexibility and Oligomeric State. *Biochemistry 53*, 1350−1359.
(30) Pelikan, M., Hura, G. L., and Hammel, M. (2009) Structure and flexibility within proteins as identified through small angle X-ray scattering. *Gen. Physiol. Biophys. 28*, 174−189.
(31) Riveros-Rosas, H., Gonzalez-Segura, L., Julian-Sanchez, A., Diaz-Sanchez, A. G., and Munoz-Clares, R. A. (2013) Structural determinants of substrate specificity in aldehyde dehydrogenases. *Chem.-Biol. Interact. 202*, 51−61.
(32) Brünger, A. T., Adams, P. D., Clore, G. M., DeLano, W. L., Gros, P., Grosse-Kunstleve, R. W., Jiang, J. S., Kuszewski, J., Nilges, M., Pannu, N. S., Read, R. J., Rice, L. M., Simonson, T., and Warren, G. L. (1998) Crystallography & NMR system: A new software suite for macromolecular structure determination. *Acta Crystallogr., Sect. D: Biol. Crystallogr. D54*, 905−921.
(33) Koncitikova, R., Vigouroux, A., Kopecna, M., Andree, T., Bartos, J., Sebela, M., Morera, S., and Kopecny, D. (2015) Role and structural characterization of plant aldehyde dehydrogenases from family 2 and family 7. *Biochem. J. 468*, 109−123.
(34) Srivastava, D., Singh, R. K., Moxley, M. A., Henzl, M. T., Becker, D. F., and Tanner, J. J. (2012) The Three-Dimensional Structural Basis of Type II Hyperprolinemia. *J. Mol. Biol. 420*, 176−189.
(35) Perez-Miller, S. J., and Hurley, T. D. (2003) Coenzyme isomerization is integral to catalysis in aldehyde dehydrogenase. *Biochemistry 42*, 7100−7109.
(36) Koppaka, V., Thompson, D. C., Chen, Y., Ellermann, M., Nicolaou, K. C., Juvonen, R. O., Petersen, D., Deitrich, R. A., Hurley, T. D., and Vasiliou, V. (2012) Aldehyde dehydrogenase inhibitors: a comprehensive review of the pharmacology, mechanism of action, substrate specificity, and clinical application. *Pharmacol. Rev. 64*, 520−539.
(37) Lamb, A. L., and Newcomer, M. E. (1999) The structure of retinal dehydrogenase type II at 2.7 A resolution: implications for retinal specificity. *Biochemistry 38*, 6003−6011.
(38) Bordelon, T., Montegudo, S. K., Pakhomova, S., Oldham, M. L., and Newcomer, M. E. (2004) A disorder to order transition accompanies catalysis in retinaldehyde dehydrogenase type II. *J. Biol. Chem. 279*, 43085−43091.
(39) Vogt, A. D., and Di Cera, E. (2013) Conformational selection is a dominant mechanism of ligand binding. *Biochemistry 52*, 5723−5729.

DOI: 10.1021/acs.biochem.5b00754
Biochemistry 2015, 54, 5513−5522